# $\beta$-delayed deuteron emission from $^6$He

D. Anthony,[1,*] L. Buchmann,[2] P. Bergbusch,[1,†] J. M. D'Auria,[1] M. Dombsky,[1,†] U. Giesen,[2,‡] K. P. Jackson,[2] J. D. King,[3] J. Powell,[3,§] and F. C. Barker[4]

[1]*Department of Chemistry, Simon Fraser University, Burnaby, British Columbia, Canada V5A 1A7*

[2]*TRIUMF, 4004 Wesbrook Mall, Vancouver, British Columbia, Canada V6T 2A3*

[3]*Department of Physics, University of Toronto, Toronto, Ontario, Canada M5S 1A7*

[4]*Department of Theoretical Physics, Research School of Physical Sciences and Engineering, Australian National University, Canberra, Australian Capital Territory 0200, Australia*

(Received 19 September 2001; published 19 February 2002)

The $\beta$ delayed deuteron decay of $^6$He has been measured at the TISOL facility at TRIUMF. For the $\beta$-particle measurement a silicon-germanium telescope array has been used. To separate deuterons from $\alpha$ particles and to obtain the spectral form of the deuteron decay, a $d$-$\alpha$ coincidence technique has been employed using two opposite silicon detectors. The $\beta$ branch has been determined from the geometry of the experiment and also by comparison with the well-known $\beta$-$\alpha$ decay modes of $^{16}$N and $^8$Li. A branching ratio of $(1.8 \pm 0.9)\times 10^{-6}$ above the $\beta$ cutoff (350-keV deuteron laboratory energy) and $(2.6\pm 1.3)\times 10^{-6}$ for the entire spectrum has been determined for this decay. In the course of the measurement the half-life of $^6$He has been remeasured to be $T_{1/2}=0.810\pm 0.008$ s. High statistical accuracy in the deuteron spectrum has been obtained that allowed a comparison of the shape of the deuteron spectrum to theoretical predictions.

DOI: 10.1103/PhysRevC.65.034310 PACS number(s): 23.40.−s, 23.20.Lv, 27.20.+n

## I. INTRODUCTION

The decay of $^6$He ($T_{1/2}=807$ ms) has been well studied for its strong ground state to ground state Gamow-Teller (GT) $\beta$ transition [1]. It has also been found [2,3] that $^6$He decays weakly by $\beta$-delayed deuteron emission, namely,

$$^6\mathrm{He}\rightarrow {}^6\mathrm{Li}^*\rightarrow {}^4\mathrm{He}+{}^2\mathrm{H}. \quad (1)$$

This is of some interest not only because this is the only reported case of such deuteron emission, but also because the $^6$He nucleus has been the focus of considerable attention as a candidate nucleus for having a neutron halo or skin.

Various theoretical reports have suggested that both the observed branching ratio and the observed particle energy spectra could be of value in understanding the structure of this interesting nuclide [4–8]. Unfortunately, the two previous determinations [2,3] of this rare decay mode are not consistent with respect to the measured branching ratio, and the published particle energy spectra lack the statistical accuracy necessary for a conclusive theoretical interpretation.

In the present paper, the branching ratio of the $\beta$-delayed deuteron decay has been remeasured and a deuteron spectrum with much higher statistics has been obtained. In addition, the half-life of $^6$He has been redetermined.

## II. EXPERIMENTAL DETAILS

### A. $^6$He production and implantation

An ion beam of the radionuclide $^6$He was produced using the thick target, on-line isotope separator TISOL located at the TRIUMF cyclotron facility in Vancouver, Canada [9–11]. A thick target (48 cm) of graphite powder was bombarded with 500-MeV protons. With the target heated to about 1500 °C, helium diffused into an ECR (electron cyclotron resonance) ion source. Singly charged $^6$He ions were extracted at 12 keV, mass analyzed ($M/\Delta m\approx 500$), passed through a 8-mm collimator and the resultant beam deposited onto a thin graphite collector (35 $\mu$g cm$^{-2}$ to allow full stopping of all beam particles). The $^6$He beam had an intensity of $10^7$ particles/(s $\mu$A) of production protons with the proton beam on target being 1 $\mu$A or slightly above.

The carbon implantation foils were mounted on aluminum cards, positioned on a rotatable wheel. Three separate detector stations were located at successive 90° intervals from the ion implantation position. The wheel was designed to rotate the $^6$He implanted foil from the collection position through to each detector position before being reexposed to the ion beam. At any given time one foil was being implanted with activity while decay events from the other three foils were recorded at each detector station. In general, the wheel holding time at the implantation/detection positions was set at about 1.1 s while the time interval for each rotation was between 0.2 and 0.25 s. Therefore, only the first detector station after rotation from the $^6$He implantation yielded particle numbers with high statistics.

### B. Detector systems

Figure 1 presents a schematic representation of the collection and detector arrangement (more details on the collector device can be found in Ref. [12]). At each of the three detector stations, each of them 90° apart (only the first one is shown in Fig. 1), the $^6$He sample was rotated between a pair of coaxial, opposite facing, charged particle Si detectors. At

*Present address: Georgetown University, Washington, D.C.

†Present address: TRIUMF, Vancouver, BC, Canada.

‡Present address: University of Notre Dame, Notre Dame, IN.

§Present address: Lawrence Berkeley Laboratory, Berkeley, CA.

 

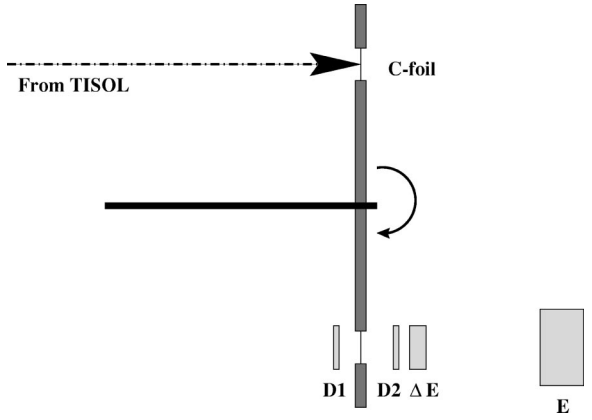


FIG. 1. Schematic setup of this experiment. The carbon collector foil is mounted on a wheel and moved periodically. $D1$ and $D2$ label the thin silicon detector for $\alpha$ and $d$ detection, $\Delta E$ and $E$ label the $\beta$ telescope. Distances in the drawing do not necessarily scale with the dimensions of the setup.

the first detection station, these were thin (10.6 $\mu$m [$D1$] and 30 $\mu$m [$D2$], 50 mm$^2$) Si surface barrier detectors with their thicknesses chosen to preferentially detect low energy $\alpha$ and deuteron particle events in the presence of the high intensity $\beta$ field. In fact, the setup of the inner detectors is identical to those of Ref. [13] (Fig. 2 there). The distances were $5.54 \pm 0.90$ mm for $D1$ and $5.35 \pm 0.22$ mm for $D2$, respectively, from the central foil position, the difference in error resulting from the respective accessibility of the detectors.

In addition to the particle detectors, the first particle detection position (which is the only one used in the analysis) housed a $\beta$ telescope consisting of a thick (500 $\mu$m) surface barrier Si detector ($14.48 \pm 0.30$ mm distance) and a 1-cm-thick Ge crystal mounted to the liquid nitrogen trap [13] at a distance of $42.20 \pm 1.1$ mm.

### C. Electronics

Energy and timing signals were generated from all detectors using standard electronics, some of them CAMAC based. Signals passing preset pulse height (energy) windows in any of the thin particle detectors were used as a master start for particle events, with a veto based upon wheel movement and computer busy to eliminate noise effects. Events were processed on an event by event basis for subsequent analysis.

Signals in the $\Delta E$ and $E$ components of the $\beta$ telescope were generated in a similar fashion and also generated a trigger in the CAMAC based data acquisition system. This was done by a hardware coincidence between the $\Delta E$ and $E$ $\beta$ detectors producing valid $\beta$ events as triggers along with recording the energy response. For the $^6$He and $^{16}$N runs the $\beta$ events were prescaled by a factor of 100; the event rate before prescaling was of the order of $10^3$ s$^{-1}$.

A precision pulser was used to monitor detector drift and gain changes for all experimental runs. In addition, pileup with $\beta$ particles will lead to a high energy tail of the pulser peak. While such a tail was observed, its magnitude is negligible.

### D. Radioactive beam purity and the half-life of $^6$He

Given the nature of the experiment it is important that the presence of any $\beta$ emitting isotopes other than $^6$He be very low. The purity of the collected ion beam was studied by measuring the activity of the collected $\beta$ particles as a function of time. The observed half-life was $T_{1/2} = 0.810 \pm 0.008$ s in excellent agreement with the literature value of $0.8067 \pm 0.0015$ s [1]. In addition, during all studies the holding time of the wheel at any position was set such that the detectors in the last positions monitored any long lived $\beta$-delayed particle activities during actual data taking. There were no $\beta$-delayed particle emitters present except for $^6$He (see Sec. III B).

The entire detection system was mounted in a vacuum chamber (pressure $\approx 10^{-6}$ Torr). The presence of a cold trap in front of the collection foil minimized any carbon deposits on the collection foils.

## III. DATA ANALYSIS I: THE PARTICLE SPECTRA AND NUMBER OF DEUTERONS

### A. Energy Calibration of particle spectra

Neither the low energy $\alpha$ particle nor the deuteron spectrum can be calibrated using known radioactive sources. Therefore, the following procedure was chosen: Careful SRIM [14] calculations were performed both for mapping the implantation profile of the $^6$He ions as well as to calculate the energy loss of $\alpha$ particles and deuterons in the carbon collection foil and the dead layer (Au) of the detectors. Then these calculations were used to determine the energy deposited from the $\beta$-delayed $\alpha$ particles emanating from $^{18}$N (1.081 and 1.409 MeV) as well as a $^{148}$Gd source (3.182 MeV). The energy loss calculations gave a deviation from linearity between these three lines that agreed with expectation. For the thin (10 $\mu$m) detector $D1$ this cross check was not possible, because the $\alpha$ particle from the $^{148}$Gd source broke through the active layer. The continuous deuteron and $\alpha$ spectra were then calibrated using the source lines corrected for energy losses and the actual calculated energy losses (foil and dead layer) at a given energy.

### B. Particle spectra and deuteron numbers

The final deuteron and $\alpha$ spectra were produced in a similar way as described in Ref. [13], i.e., coincidences between the deuteron and the recoiling $\alpha$ particle were recorded. Contour plots of the resulting $D1$-$D2$ coincidence spectrum are shown in Fig. 2. Clearly, $d$-$\alpha$ and $\alpha$-$d$ coincidences are separated down to an energy where the $\beta$ background, induced by random coincidence events, becomes overwhelming. In a similar manner to Ref. [13] a ratio cut can be made on the coincidence spectra and single deuteron or $\alpha$ spectra can be derived. The deuteron spectrum recorded in detector $D2$ is shown in Fig. 3. $\beta$-induced background becomes dominant for a center-of-mass (c.m.) energy below 400 keV.

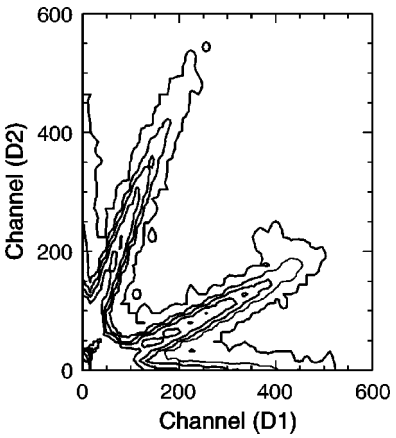


FIG. 2. Contour plot of the coincidence spectrum between detectors $D1$ and $D2$. The lowest contour levels are for 1, 20, 50, 100, and 200 events, respectively.

The shape of this background contribution is determined by making a cut at a high ratio where no $d$-$\alpha$ coincidence events are present. It is consistent with a decaying exponential function. For an initial estimation of the branching ratio, a cut was placed at 350-keV deuteron laboratory energy (525-keV cm energy), above which the $\beta$-induced background is small. In 12 runs 4468 deuteron events were recorded in detector $D1$ and 4316 events in detector $D2$ above this energy. High energy deuterons, however, penetrated through the active layer of detector $D1$, making the spectrum unsuitable for fits.

Any contaminants from $\beta$-delayed particle emitters other than $^6$He should show at different ratio lines than the ones for $^6$He in Fig. 2. In addition, there are no known $\beta$-delayed particle emitters other than $^6$He whose maximum experimental decay energy is only about 1 MeV. Any known $\beta$-delayed particle emitter should show higher energy events than are present in the data.

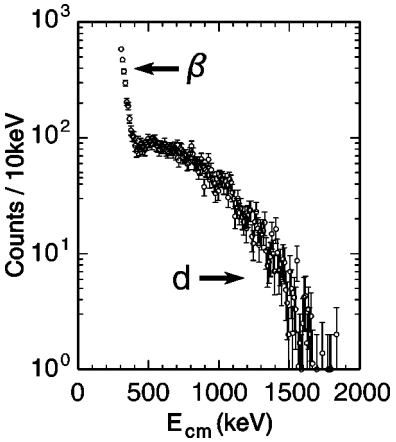


FIG. 3. Deuteron spectrum as recorded in detector $D2$ in $\alpha$ coincidence with $D1$. An energy calibration as described in the text is applied.

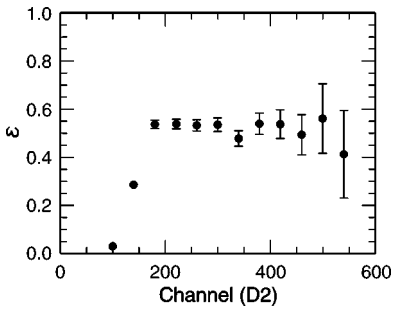


FIG. 4. Ratio $\epsilon$ of single to coincidence spectrum counts for 40 ADC channels integrated for one of the data collection runs (detector $D2$).

## IV. DATA ANALYSIS II: RELATIVE EFFICIENCIES AND THE $\beta$-DEUTERON BRANCHING RATIO

### A. Efficiency calibrations for the $\beta$-particle branching ratio

The branching ratio (BR) has been determined using the expression

$$\mathrm{BR}=\frac{N_d\epsilon_\beta}{N_\beta\beta_{con}\epsilon_d\epsilon_c}, \tag{2}$$

where $N_d$ is the number of detected deuterons (above 350 keV), $\epsilon_\beta$ the efficiency for $\beta$ detection, $N_\beta$ the number of detected $\beta$ particles, $\beta_{con}$ the $\beta$ conversion factor, i.e., the ratio of total $\beta$ particles to above threshold $\beta$ particles, $\epsilon_d$ the efficiency for the deuteron detection, and $\epsilon_c$ the coincidence efficiency of detected deuterons relative to single events. Therefore, several efficiencies or ratios of efficiencies needed to be determined, in particular $\beta_{con}$, $\epsilon_\beta/\epsilon_d$, and $\epsilon_c$.

The $\beta$ particles were detected in coincidence between a Si $\Delta E$ detector of 500 $\mu$m thickness and an $E$ Ge counter of 1 cm thickness. For noise and count rate reasons a lower detection threshold was present. This threshold was determined from energy loss calculations of the $\beta$ particles for the $\Delta E$ detector and the energy calibration of the Ge detector via $\gamma$ sources. The $\beta$-detection threshold was determined to be at $810\pm100$ keV. Employing the theoretical form of the $\beta$ spectrum, $\beta_{con}$ was found to be $2.02\pm0.32$ for $^6$He.

The $\alpha$ particles and the deuterons were distinguished by using a recoil coincidence technique as described in Ref. [13] and discussed in Sec. III B. While the coincidence between the $\alpha$ particle and the deuteron is kinematically enforced, the coincidence efficiency is less than the single detection efficiency for each particle for solid angle reasons. However, the ratio between the single detection efficiency and the coincidence detection efficiency can be relatively easily determined by taking the ratio of the number of events above the $\beta$-noise and $\alpha$-particle level[1] in each run for single and coincidence events. This is similar to the procedure applied in Ref. [13], Fig. 11 there. Other coincidence efficiency tests of Ref. [13] also apply for this experiment. Figure 4 shows the

[1]Low energy $\alpha$ particles are shifted downward in pulse height relative to deuterons.

ratio of coincidence and single events for one of the runs for 40 analog-to-digital converter (ADC) channels integrated. It shows that the coincidence efficiency stays constant down to an ADC channel of about 200; below this channel the single spectrum $\beta$ tail lowers the ratio. Only data where the coincidence efficiency was known, i.e., above 350 keV in the center-of-mass system, were used in the analysis, see Sec. III B. The coincidence efficiency was determined for each run; a table of the coincidence efficiency for each relevant run can be found in Ref. [12] of the 12 runs used in the final analysis. The coincidence efficiency $\epsilon_c$ and the detected deuteron number show some correlation, while their respective ratio stays constant. This indicates some fluctuations in the implantation position, see Sec. IV C.

The efficiency ratio $\epsilon_\beta/\epsilon_d$ has been determined in two principal ways: (i) by calculating the solid angle of the entire detection system, and (ii) by using the known $\beta$-particle branching ratios of $^8$Li and $^{16}$N. The solid angle calculation shows that the smaller solid angle of the $E$ detector dominates the result for the $\beta$ detection. For detectors $D1$ and $D2$ the coincidence efficiency ratio $\epsilon_\beta/\epsilon_d$ is found to be $0.11 \pm 0.05$ and $0.11 \pm 0.02$, because detector $D2$ (with the smaller error) is more easily accessible, see Sec. II B.

The source method required that the ratio of accepted to total number of $\beta$ particles $\beta_{con}$ was calculated from a theoretical spectrum as described above for the two reference isotopes. For the decay of $^{16}$N the dominant decays to the ground state and the second excited state of $^{16}$O were taken into account ($\beta_{con}=1.33\pm0.18$). The $\beta$-$\alpha$ branching ratio of Ref. [15] $(1.2\pm0.05)\times10^{-5}$ was used. With this the ratio $\epsilon_\beta/\epsilon_d$ is found to be $0.078\pm0.019$ and $0.111\pm0.028$ for detectors $D1$ and $D2$, respectively.

Because the ECR source was used in the runs, $^8$Li was implanted into the collector foil using $^8$He ions [$T_{1/2}(^8\mathrm{He})=0.119$ s, $T_{1/2}(^8\mathrm{Li})=0.8403$ s]. Decay curves were taken and after an appropriate time the then largely $^8$Li decay was sampled. Corrections for possible $^8$He $\beta$ events were applied, in addition. $\beta_{con}$ was determined to be $1.04\pm0.01$ because of the high $\beta$-decay $Q$ value of $^8$Li. Then $\epsilon_\beta/\epsilon_d$ is found to be $0.093\pm0.009$ and $0.140\pm0.015$ for detectors $D1$ and $D2$, respectively.

While the deviations between these three determinations of the efficiency ratio $\epsilon_\beta/\epsilon_d$ is at the most on the $2\sigma$ level, it is most prudent to treat them as three independent measurements irrespective of their (smaller than the deviations) individual errors and include all measurements within one standard deviation. Then for $D1$: $\epsilon_\beta/\epsilon_d=0.094\pm0.017$, and for detector $D2$: $\epsilon_\beta/\epsilon_d=0.120\pm0.020$.

The total number of $\beta$ particles detected in the 12 runs was $N_\beta=2.8873\times10^8$. Individual runs were, however, evaluated separately.

### B. $\beta$-$d$ branching ratio above the $\beta$ cutoff

To calculate the branching ratio (Eq. 2) all 12 runs were evaluated. With the errors added in quadrature, the total, efficiency corrected, number of $\beta$ decays is calculated to be $(23.4\pm5.6)\times10^8$ and $(23.8\pm5.5)\times10^8$ for detectors $D1$ and $D2$, respectively, both numbers being highly correlated. This gives branching ratios for deuterons with energy above the $\beta$-noise cutoff of 350 keV $(1.9\pm0.5)\times10^{-6}$ and $(1.8\pm0.4)\times10^{-6}$. Averaging and using the most conservative assumption, we obtain $(23.6\pm5.8)\times10^8$ as the total number of $\beta$ decays and $(1.8\pm0.5)\times10^{-6}$ as the branching ratio above 350 keV of deuteron energy.

### C. Systematic errors

Systematic errors were evaluated by varying the best values of the parameters that determine the branching ratio. These systematic errors include the $\beta$-detection threshold, random coincidences between the particles, several geometric effects such as variation in the implantation point and the beam spot diameter, variations in the foil positioning between the detectors, and possible nonlinearities in the particle energy calibration [12]. The largest errors found for both $D1$ and $D2$ are resulting from the $\beta$-detection threshold $(0.4\times10^{-6})$ and geometrical factors $(0.5\times10^{-6})$. With all errors added in quadrature, the systematic error in the branching ratio is found to be $0.7\times10^{-6}$. The final branching ratio above 350 keV (laboratory) is then $(1.8\pm0.9)\times10^{-6}$. This is appreciably less than the previously reported value of $(7.6\pm0.6)\times10^{-6}$ [3], which superseded the earlier value of $(2.8\pm0.5)\times10^{-6}$ [2] for deuterons above 250 keV.

## V. *R*-MATRIX FITS AND THE TOTAL $\beta$-PARTICLE BRANCHING RATIO

In Ref. [16], the branching ratio and deuteron spectrum measured in Ref. [3] were reproduced in an *R*-matrix calculation that included both internal and external contributions to the GT matrix element. We use the same approach to fit the present data, using formulas from Ref. [16]. The deuteron spectrum is given by the one-level ($^6$Li ground state), one-channel ($^4\mathrm{He}+d, l=0$) approximation of *R*-matrix theory,

$$N(E)=f_\beta(E)P_0(E)\times\frac{B_{1G}^2(E)\,\gamma_{1d}^2}{[E_1-\gamma_{1d}^2\{S_0(E)-B_0\}-E]^2+[\gamma_{1d}^2P_0(E)]^2}, \tag{3}$$

where the GT matrix element $B_{1G}(E)$ is a function of the c.m. energy $E$, due to the inclusion of the contribution from the channel region ($r>a$, where $a$ is the channel radius). It can be written as

$$B_{1G}(E)=c_1\frac{1+c_2\frac{1}{a}\int_a^\infty E_i(r)E_f(E,r)dr}{[1+\gamma_{1d}^2 dS_0(E)/dE]^{1/2}}, \tag{4}$$

where $E_i(r)$ and $E_f(E,r)$ are radial wave functions for the initial and final states, normalized to unity at $r=a$. The parameter $c_2$ is defined by

$$c_2 = 2\theta_i \theta_f m_{if}/M_{if}, \tag{5}$$

where $\theta_i$ and $\theta_f$ are the dimensionless reduced width amplitudes of the initial $^6$He and final $^6$Li states, $m_{if}$ is the GT matrix element for a $2n$ to $d$ transition, and $M_{if}$ is the internal part of the GT matrix element for the $^6$He to $^6$Li transition. The constant $c_1$ is determined by fitting the total number of $\beta$ decays. The two remaining parameters are $c_2$ and $\theta_f^2$. In Ref. [16], these were chosen to fit the measured branching ratio and the $^4$He$+d$ $s$-wave phase shift at a particular energy. As the internal and external contributions to the GT matrix element are of opposite sign for $E>0$, there are, for each value of $a$, two solutions for $c_2$ corresponding to the internal contribution being greater than [case (a)] or less than [case (b)] the external contribution. The deuteron spectrum of Ref. [3] was not sufficiently precise to allow a clear preference for (a) or (b), or for a particular value of $a$. The present deuteron spectrum has better statistics, and makes possible a least-squares determination of the parameter values. The normalization of the $\beta$-background contribution (which is a decaying exponential function)is taken as an additional adjustable parameter. The fit is made to the spectrum with $E \geqslant 0.365$ MeV. Also, included in the fit are values of the $^4$He$+d$ $s$-wave phase shift taken from Ref. [17], for $E=2.00$–$3.89$ MeV, with arbitrarily assigned errors of $\pm 3°$.

The best fit is found for case (a) with $a=4.14$ fm, with the parameter values $\theta_f^2=0.0559$ and $c_2=0.0509$ and a total $\chi^2$ value of 113 for the deuteron spectrum (148 data points). The fits to the deuteron spectrum (with background subtracted) and to the phase shift are shown by the solid curves in Figs. 5(a) and 5(b). Integrating over the whole deuteron spectrum and allowing for the uncertainty in the total number of decays gives the branching ratio for $^6$He $\beta$-delayed deuteron emission as $(2.6\pm 1.3)\times 10^{-6}$ with the error scaled from the branching value above 350 keV. The error resulting from the extrapolation of the spectrum is expected to be small compared to the other errors.

The parameter $\xi$ introduced in Ref. [3] can be written as

$$\xi = \frac{\theta_i}{\theta_f}\frac{m_{if}}{M_{if}} = \frac{c_2}{2\theta_f^2}, \tag{6}$$

so that the present fit gives $\xi=0.455$. The $^6$Li spectroscopic factor $S_f$ may be calculated from Eq. (21) of Ref. [16], with the single-particle dimensionless reduced width evaluated for a Woods-Saxon potential (as given in Ref. [4]); this gives $S_f=0.090$. Experimental values of $S_f$ obtained in other ways are much larger than this; e.g., $0.85\pm 0.04$ from $^4$He$(d,\gamma)^6$Li [18], 0.42 from $^4$He$(d,d)^4$He [18], and 0.76–0.84 from $^6$Li$(p,pd)^4$He [19].

Values of $S_f$ from fits to the present data are somewhat larger for larger values of $a$; e.g., for $a=4.5$ fm, one obtains $S_f=0.116$. This fit is shown by the dashed curves in Figs. 5(a) and 5(b). The fit to the spectrum is almost identical to the best fit, whereas the fit to the phase shifts of Ref. [17] is much poorer; it agrees well with the earlier phase shift values from Ref. [20], which are also shown in Fig. 5(b). A larger value of $S_f$ might be possible, if contributions from the 5.65 MeV $1^+$ level of $^6$Li were included; these could be significant for the phase shift, but would not be expected to be important for the deuteron spectrum, because the GT matrix element for this state is calculated to be very small. As $\theta_f^2$ is roughly proportional to the branching ratio, the low value of $S_f$ obtained here may be attributed at least in part to the small value of the branching ratio.

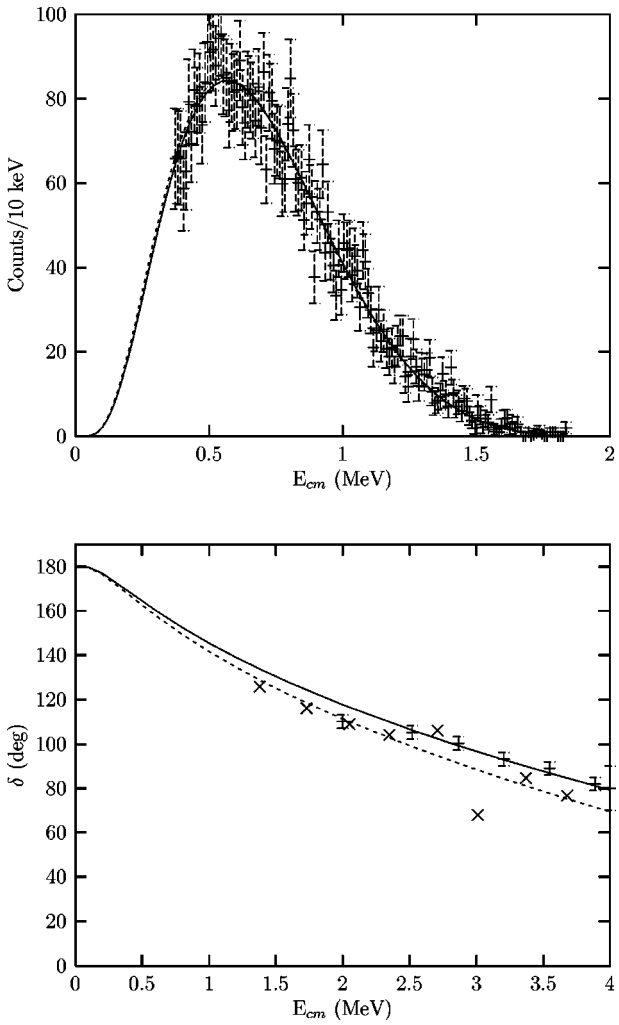


FIG. 5. (a) Deuteron spectrum as a function of c.m. energy. The experimental points are from the data in detector $D2$ after subtraction of an exponential background determined in a simultaneous $R$-matrix fit to these data and to the $^4$He$+d$ $s$-wave phase shift data from Ref. [17]. The curves are the best fits for $a=4.14$ fm (solid) and 4.5 fm (dashed). (b) $^4$He$+d$ $s$-wave phase shift as a function of c.m. energy. The experimental points are from Ref. [17] (bars) and Ref. [20] (crosses). The curves are as in (a).

## VI. CONCLUSIONS

In the present experiment a $d$-$\alpha$ branching ratio of $(1.8\pm 0.9)\times 10^{-6}$ has been measured above a deuteron energy of 350 keV using most conservative error estimates. Applying $R$-matrix theory, a total branching ratio of $(2.6\pm 1.3)\times 10^{-6}$ has been found. In Ref. [3] a branching ratio of

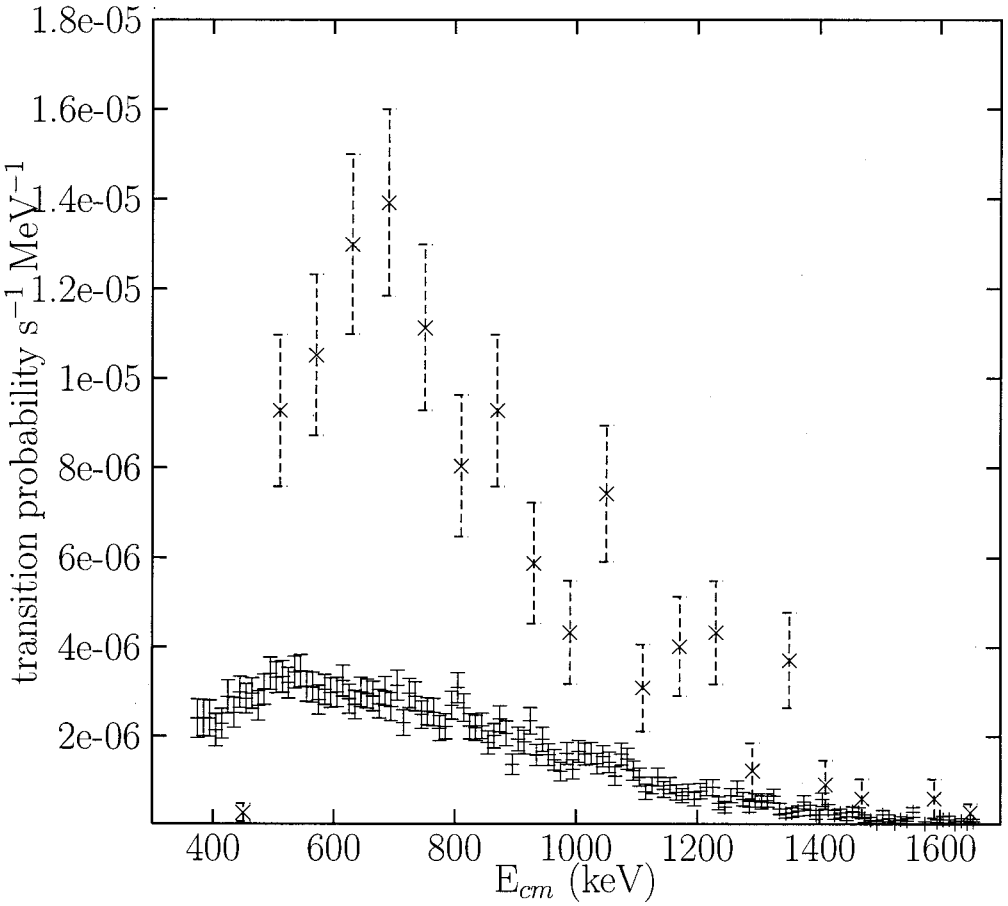


FIG. 6. Comparison of the present deuteron spectrum (straight line) with the one of Ref. [3] (cross). Data points of Ref. [3] have assigned errors of statistical nature only.

$(7.6\pm0.6)\times10^{-6}$ is given that is inconsistent with the present paper. A comparison of both spectra is shown in Fig. 6.

There have been several calculations of the $\beta$-delayed deuteron spectrum from $^{6}$He, using potential and microscopic cluster models [4–8]. Most have obtained branching ratios greater than those found here. In best agreement with the present branching ratio for $E>525$ keV is the value of $3.1\times10^{-6}$ given in Ref. [7]. In most of these calculations the deuteron spectrum has a maximum at an energy of 0.3 to 0.4 MeV, whereas the present data and *R*-matrix fit to the data peak at 0.57 MeV. Consequently, Ref. [7] finds a total branching ratio of $6.0\times10^{-6}$, which is appreciably greater than the one found here, while the higher energy part would lead to a comparable branching ratio with the present one.

## ACKNOWLEDGMENTS

The authors wish to thank TRIUMF's operational and technical staff for their collaboration. The help of P. Machule, H. Sprenger, and H. Biegenzein in the course of the experiment is gratefully acknowledged.

[1] D. R. Tilley, C. M. Cheves, J. L. Godwin, G. M. Hale, H. M. Hoffman, J. H. Kelley, and H. R. Weller, Energy Levels of Light Nuclei, $A=6$, preprint, 2001; www.tunl.duke.edu/NuclData/

[2] K. Riisager, M. Borge, H. Gabelmann, P. Hansen, L. Johannsen, B. Johnson, W. Kircewicz, G. Nyman, A. Richter, O. Tengblad, and K. Wilhelmsen, Phys. Lett. B **235**, 30 (1990).

[3] M. Borge, L. Johannsen, B. Johnson, T. Nilson, G. Nyman, K. Riisager, O. Tengblad, and K. Wilhelmsen Rolander, Nucl. Phys. **A560**, 664 (1993).

[4] P. Descouvement and C. Leclerq-Villain, J. Phys. G **18**, L99 (1992).

[5] M. Zhukov, B. Danilin, L. Grigorenko, and N. Shul'gina, Phys. Rev. C **47**, 2937 (1993).

[6] D. Baye, Y. Suzuzki, and P. Descouvement, Prog. Theor. Phys. **91**, 271 (1994).

[7] A. Csoto and D. Baye, Phys. Rev. C **49**, 818 (1994).

[8] K. Varga, Y. Suzuki, and Y. Ohbayashi, Phys. Rev. C **50**, 189 (1994).

[9] M. Dombsky, J.M. D'Auria, L. Buchmann, H. Sprenger, J. Vincent, P. McNeely, and G. Roy, Nucl. Instrum. Methods Phys. Res. A **295**, 291 (1990).

[10] L. Buchmann, J. Vincent, H. Sprenger, M. Dombsky, J.M. D'Auria, P. McNeely, and G. Roy, Nucl. Instrum. Methods Phys. Res. B **62**, 521 (1992).

[11] M. Dombsky, L. Buchmann, J.M. D'Auria, H. Sprenger, P.

McNeely, G. Roy, H. Sprenger, and J. Vincent, Nucl. Instrum. Methods Phys. Res. B **70**, 125 (1992).

[12] D. Anthony, Master thesis, Simon Fraser University, Burnaby, Canada, 1995.

[13] R.E. Azuma, L. Buchmann, F.C. Barker, C.A. Barnes, J.M. D'Auria, M. Dombsky, U. Giesen, K.P. Jackson, J.D. King, R.G. Korteling, P. McNeely, J. Powell, G. Roy, J. Vincent, T.R. Wang, S.S.M. Wong, and P.R. Wrean, Phys. Rev. C **50**, 1194 (1994).

[14] J. F. Ziegler and J. P. Biersack, *The Stopping Power and Range of Ions in Solids* (Pergamon, New York, 1990).

[15] H. Hättig, K. Hünchen, and H. Wäffler, Phys. Rev. Lett. **25**, 941 (1970); K. Neubeck, H. Schober, and H. Wäffler, Phys. Rev. C **10**, 320 (1974).

[16] F.C. Barker, Phys. Lett. B **322**, 17 (1994).

[17] W. Grüebler, P.A. Schmelzbach, V. König, R. Risler, and D. Boerma, Nucl. Phys. **A242**, 265 (1975).

[18] R.G.H. Robertson, P. Dyer, R.A. Warner, R.C. Melin, T.J. Bowles, A.B. McDonald, G.C. Ball, W.G. Davies, and E.D. Earle, Phys. Rev. Lett. **47**, 1867 (1981).

[19] R.E. Warner, R.S. Wakeland, J.Q. Yang, D.L. Friesel, P. Schwandt, G. Caskey, A. Galonsky, B. Remington, and A. Nadasen, Nucl. Phys. **A422**, 205 (1984); R.E. Warner, J.Q. Yang, D.L. Friesel, P. Schwandt, G. Caskey, A. Galonsky, B. Remington, A. Nadasen, N.S. Chant, F. Khuzaie, and C. Wang, *ibid.* **A443**, 64 (1985).

[20] L.C. McIntyre and W. Haeberli, Nucl. Phys. **A91**, 382 (1967).